Analytical and numerical prediction of acoustic radiation from a panel under turbulent boundary layer excitation

M. Karimi, Laurent Maxit, P. Croaker, O. Robin, A. Skvortsov, S. Marburg, N. Atalla, N. Kessissoglou

Analytical and numerical prediction of acoustic radiation from a panel under turbulent boundary layer excitation

M. Karimi[1*], L. Maxit[2], P. Croaker[3], O. Robin[4],
A. Skvortsov[3], S. Marburg[5], N. Atalla[4], N. Kessissoglou[6]

[1] *Centre for Audio, Acoustics and Vibration, University of Technology Sydney, Sydney, Australia*

[2] *Univ Lyon, INSA–Lyon, Laboratoire Vibrations-Acoustique (LVA), 25 bis, av. Jean Capelle, F-69621, Villeurbanne Cedex, France*

[3] *Maritime Division, Defence Science and Technology, Melbourne, Australia*

[4] *Groupe d'Acoustique de l'Université de Sherbrooke, Université de Sherbrooke, Sherbrooke, J1K 2R1, Canada*

[5] *Chair of Vibroacoustics of Vehicles and Machines, Department of Mechanical Engineering, Technische Universität München, München, Germany*

[6] *School of Mechanical and Manufacturing Engineering, UNSW Sydney, Australia*

Abstract

The vibroacoustic responses of a simply supported panel excited by turbulent flow are analytically and numerically investigated. In the analytical model, the radiated sound power is described in terms of the cross spectrum density of the wall pressure field and sensitivity functions for the acoustic pressure and fluid particle velocity. For the numerical model, a hybrid approach based on the finite element method is described in which the cross spectrum of the wall pressure field is represented by a set of uncorrelated wall plane waves. Realisations of the wall pressure field are used as deterministic input loads to the panel. The structural and acoustic responses of the panel subject to turbulent boundary layer excitation are then obtained from an ensemble average of the different realisations. Analytical and numerical results are compared with experimental data measured in an anechoic wind tunnel, showing good agreement. The effect of adding stiffeners on the vibroacoustic responses of the panel is also examined using the proposed

*Corresponding author
Email address: Mahmoud.karimi@uts.edu.au

numerical approach.

Keywords: turbulent boundary layer, acoustic radiation, wall pressure field, uncorrelated wall plane waves

1. INTRODUCTION

The vibroacoustic responses (i.e., the structural and acoustic responses) of elastic structures excited by the pressure field beneath a turbulent boundary layer (TBL) are a significant concern in naval and aircraft industries. An extensive number of analytical and numerical approaches as well as experiments have been conducted to predict the vibroacoustic responses of planar structures excited by turbulent flow, for example, see Refs. [1–8]. The structural responses of elastic panels excited by a turbulent flow or an acoustic diffuse field have been recently reviewed by the authors [9]; as such we herein concentrate on the acoustic responses of elastic panels excited by turbulent flow. The radiated sound power from a thin panel in air excited by a TBL was computed by Davies [10] using both deterministic and statistical methods. In the deterministic method, an estimation of the radiated sound power was obtained by summing over resonant modes from a modal analysis. Statistical Energy Analysis was also employed to predict the radiated power. Results from the two methods were shown to converge at frequencies above the hydrodynamic coincidence frequency. Han et al. [11] developed a hybrid computational fluid dynamics (CFD)-energy flow analysis (EFA) method to predict the vibroacoustic responses of a panel excited by turbulent flow. CFD was employed to obtain mean flow information. The travelling wave method was used to calculate the input power to the system. The structural and acoustic responses of the panel were then obtained using the EFA.

An analytical formulation in the wavenumber domain was proposed by Maury et al. [12; 13] to predict the vibroacoustic responses of a panel excited by either a diffuse acoustic field or a turbulent boundary layer. An increase in flow velocity was observed to more rapidly increase the radiated sound pressure than the turbulent pressure. Rocha [14] developed an analytical method to study the vibroacoustic responses of isotropic and composite plates under TBL excitation. It was shown that smaller composite panels generally produced lower levels of sound and vibration than longer and wider composite panels. Further, it was observed that apart from some distinct frequencies, the composite panels generated lower noise levels than that by isotropic pan-

els. Recently, Marchetto et al. [6; 15] studied the vibroacoustic responses of panels under diffuse acoustic field and TBL excitation. They used a method based on sensitivity functions and reciprocity principles. Two crucial quantities in the wavenumber domain were identified which had significant effect on the panel vibroacoustic responses. They are the wall-pressure cross spectral density function of the excitation and the sensitivity function at the receiver location. Kou et al. [16] examined the modal averaged radiation efficiency of a rectangular plate subject to TBL excitation. Below the hydrodynamic coincidence frequency, the radiation efficiency was found to increase with an increase in the convection velocity, attributed to the increase of the modal radiation efficiency associated with lower order modes.

Cousin [17] experimentally investigated sound generation from a flat plate excited on one side by turbulent flow. The sound levels were observed to increase with decreasing frequency and increasing flow speed. Results showed that the greatest radiated sound energy occurred at frequencies around and below the aerodynamic coincidence frequency. Park et al. [18] carried out an experiment to study vibration responses and the sound radiation of a viscoelastically supported rectangular plate excited by turbulent flows. The measured results were in good agreement with predictions from an analytical model described in previous publications. The vibroacoustic responses of a fluid-loaded plate were numerically and experimentally investigated by Ciappi et al. [19]. It was shown that among the TBL models considered in their work, the Chase model provided good agreement between numerical and experimental results. Liu et al. [4; 20] studied the vibroacoustic responses of aircraft panels with and without ring frame attachments excited by a TBL, using the modal expansion and receptance methods. They showed that whilst the TBL pressure field produces the same vibration level for the panel with and without ring frame attachments, the excited modes of the stiffened plate are more efficient sound radiators. They also showed that an increase in the skin loss factor dramatically reduced TBL-induced noise radiation.

In this paper, analytical and numerical approaches to predict the radiated acoustic power of an elastic panel subject to TBL excitation are presented. In the analytical model, expressions for the cross-spectrum density of the wall pressure field (WPF), and sensitivity functions for the acoustic pressure and fluid particle velocity are derived. The acoustic power is then obtained by integrating the cross spectrum between the acoustic pressure and fluid particle velocity over the panel surface. The numerical model couples an

uncorrelated wall plane wave technique which describes the WPF with a vibroacoustic solver based on the finite element method (FEM), as described previously in Refs [9; 21]. The turbulent boundary layer excitation is modelled using a set of uncorrelated wall plane waves. Each realisation of the wall pressure field is a deterministic input load to the vibroacoustic solver. The structural and acoustic responses of the panel are then obtained from an ensemble average of the different panel responses. Acoustic radiation from a simply supported panel is initially examined, from which results obtained analytically and numerically are compared with experimental data. The analytical method is limited in its application to simple panels with simply supported boundary conditions. In contrast, the numerical method can be applied to complex structures with arbitrary boundary conditions. To show one of the applications of the proposed numerical method, acoustic radiation from a stiffened panel is then numerically predicted and the results are compared with those of the unstiffened panel.

2. Analytical formulation

Figure 1 shows an elastic rectangular finite baffled panel excited by a turbulent flow field. It is assumed that the TBL is homogeneous, stationary and fully developed over the panel surface. Although in practice there are inhomogeneities in the TBL, we are considering an idealised WPF associated with the boundary layer developed on an extended flat surface in a subsonic flow with zero pressure gradient. In such a flow condition, the boundary layer thickness increases slowly in the flow direction which justifies representing the TBL as a homogeneous spatial field and stationary in time. Further, it is assumed that the WPF is not altered by the vibration of the panel. The analytical model is herein developed in the wavenumber domain.

2.1. Panel velocity

The spatial average of the auto spectrum density (ASD) of the panel velocity is given by

$$\left\langle V^2 \right\rangle = \frac{1}{A} \int_A S_{vv}(\mathbf{x}, \omega) \mathrm{d}A, \tag{1}$$

where S_{vv} is the ASD of the panel flexural velocity, $\mathbf{x}$ is a point location on the panel, ω is the angular frequency, $A = L_x L_y$ is the panel surface area and

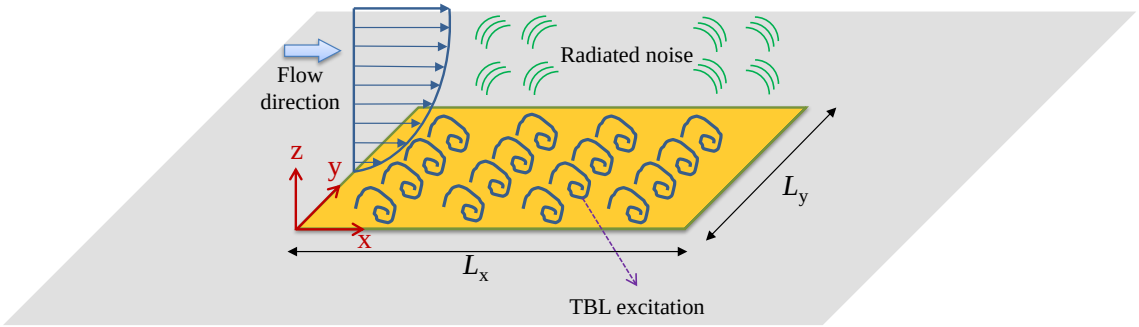

Figure 1: An elastic baffled panel under TBL excitation.

L_x, L_y are the panel length and width in the x and y directions, respectively. S_{vv} is obtained using [12; 22]

$$S_{vv}(\mathbf{x},\omega) = \frac{1}{4\pi^2}\int_{\infty} |H_{v_s}(\mathbf{x},\mathbf{k},\omega)|^2 \, \phi_{pp}(\mathbf{k},\omega)\mathrm{d}\mathbf{k}, \tag{2}$$

where $H_{v_s}(\mathbf{x},\mathbf{k},\omega)$ is the sensitivity function of the panel vibration velocity excited by a unit wall plane wave given in Appendix A. $\phi_{pp}(\mathbf{k},\omega)$ is the cross spectrum density (CSD) of the pressure field in the wavenumber domain, and $\mathbf{k}$ is the wavevector with components k_x and k_y in the streamwise and spanwise directions, respectively. Substituting equation (2) and the sensitivity function given by equation (A.1) into equation (1), and using rectangular rule for numerical integration in the wavenumber domain, the spatial average of the auto spectrum of the panel velocity can be written as follows

$$\langle V^2 \rangle \approx \frac{1}{4\pi^2}\sum_{i=1}^{N_x}\sum_{j=1}^{N_y} \phi_{pp}(\mathbf{k},\omega)\Lambda_{ij}(\mathbf{k},\omega)\delta k_x \delta k_y, \tag{3}$$

$$\Lambda_{ij}(\mathbf{k},\omega) = \sum_{m=1}^{M}\sum_{n=1}^{N}\sum_{h=1}^{M}\sum_{l=1}^{N} Z_{mn}^{ij} Z_{hl}^{ij^*} \widehat{\varphi}_{mnhl} \tag{4}$$

$$\left\{ Z_{rs}^{ij} | (r,s) = (m,n) \vee (h,l) \right\} = \frac{\mathrm{i}\omega\psi_{rs}(\mathbf{k})}{\Omega(\omega_{rs}^2 - \omega^2 + \mathrm{i}\eta\omega\omega_{rs})} \tag{5}$$

$$\widehat{\varphi}_{mnhl} = \frac{1}{A}\int_A \sin(\frac{m\pi x}{L_x})\sin(\frac{n\pi y}{L_y})\sin(\frac{h\pi x}{L_x})\sin(\frac{l\pi y}{L_y})\mathrm{d}A = \left\{ \begin{array}{ll} \frac{1}{4}, & \text{if } \ m = h \wedge n = l \\ 0, & \text{otherwise} \end{array} \right\}. \tag{6}$$

where δk_x, δk_y are the wavenumber resolutions in the streamwise and spanwise directions, respectively, and N_x, N_y are the number of points considered for sampling the wavenumber space along the k_x and k_y directions. M and N are the cut-off modal orders in the x and y directions, respectively. ψ_{rs} and ω_{rs} are the modal forces and modal angular frequencies which are defined in Appendix A, Ω is the modal mass and η is the structural loss factor. According to equation (6), $\widehat{\varphi}_{mnhl}$ is non-zero only if $m = h \wedge n = l$. This can simplify equation (4) as follows

$$\Lambda_{ij}(\mathbf{k},\omega) = \frac{1}{4}\sum_{m=1}^{M}\sum_{n=1}^{N}\left|Z_{mn}^{ij}\right|^2 \tag{7}$$

2.2. Acoustic power

The acoustic power of the panel can be obtained by integrating the normal sound intensity corresponding to the cross spectrum between the sound pressure and the fluid particle velocity, over a virtual surface Γ surrounding the panel as follows [23; 24]

$$\Pi_{\mathrm{rad}}(\omega) = \int_\Gamma \mathrm{Re}\left\{S_{pv_f}(\mathbf{x},\omega)\right\}\mathrm{d}\mathbf{x}. \tag{8}$$

The cross spectrum denoted by S_{pv_f} is given by the following analytical expression [12; 15]

$$S_{pv_f}(\mathbf{x},\omega) = \frac{1}{4\pi^2}\int_\infty H_p(\mathbf{x},\mathbf{k},\omega)H_{v_f}^*(\mathbf{x},\mathbf{k},\omega)\phi_{pp}(\mathbf{k},\omega)\mathrm{d}\mathbf{k}, \tag{9}$$

where $H_p(\mathbf{x},\mathbf{k},\omega)$, $H_{v_f}(\mathbf{x},\mathbf{k},\omega)$ are sensitivity functions for the radiated pressure and the fluid particle velocity, respectively. The sensitivity functions in

the wavenumber domain, denoted by $\tilde{H}_p(\tilde{\mathbf{k}}, \mathbf{k}, \omega)$ and $\tilde{H}_{v_f}(\tilde{\tilde{\mathbf{k}}}, \mathbf{k}, \omega)$, are related to the sensitivity functions in the spatial domain by inverse Fourier transform as follows

$$H_p(\mathbf{x}, \mathbf{k}, \omega) = \frac{1}{4\pi^2} \int_{\infty} \tilde{H}_p(\tilde{\mathbf{k}}, \mathbf{k}, \omega) e^{\mathrm{i}\tilde{\mathbf{k}}\mathbf{x}} \mathrm{d}\tilde{\mathbf{k}}, \tag{10}$$

$$H^*_{v_f}(\mathbf{x}, \mathbf{k}, \omega) = \frac{1}{4\pi^2} \int_{\infty} \tilde{H}^*_{v_f}(\tilde{\tilde{\mathbf{k}}}, \mathbf{k}, \omega) e^{-\mathrm{i}\tilde{\tilde{\mathbf{k}}}\mathbf{x}} \mathrm{d}\tilde{\tilde{\mathbf{k}}}, \tag{11}$$

where * denotes the complex conjugate. Using equations (8)-(11) and extending virtual surface Γ to infinity in the equation (8) (note that except over the panel, the fluid particle velocity is zero everywhere on the virtual surface), the radiated acoustic power becomes

$$\Pi_{\mathrm{rad}}(\omega) = \mathrm{Re}\left[\left(\frac{1}{4\pi^2} \right)^2 \int_{\infty} \int_{\infty} \int_{\infty} \tilde{H}_p(\tilde{\mathbf{k}}, \mathbf{k}, \omega) \tilde{H}^*_{v_f}(\tilde{\tilde{\mathbf{k}}}, \mathbf{k}, \omega) \phi_{pp}(\mathbf{k}, \omega) \left(\frac{1}{4\pi^2} \int_{\infty} e^{\mathrm{i}(\tilde{\mathbf{k}} - \tilde{\tilde{\mathbf{k}}})\mathbf{x}} \mathrm{d}\mathbf{x} \right) \mathrm{d}\mathbf{k} \mathrm{d}\tilde{\mathbf{k}} \mathrm{d}\tilde{\tilde{\mathbf{k}}} \right]. \tag{12}$$

The integral in the parenthesis in equation (12) corresponds to the Dirac delta function which is given by

$$\frac{1}{4\pi^2} \int_{\infty} e^{\mathrm{i}(\tilde{\mathbf{k}} - \tilde{\tilde{\mathbf{k}}})\mathbf{x}} \mathrm{d}\mathbf{x} = \delta(\tilde{\mathbf{k}} - \tilde{\tilde{\mathbf{k}}}). \tag{13}$$

Using this definition, equation (12) can be simplified to

$$\Pi_{\mathrm{rad}}(\omega) = \mathrm{Re}\left[\left(\frac{1}{4\pi^2} \right)^2 \int_{\infty} \int_{\infty} \tilde{H}_p(\tilde{\mathbf{k}}, \mathbf{k}, \omega) \tilde{H}^*_{v_f}(\tilde{\mathbf{k}}, \mathbf{k}, \omega) \phi_{pp}(\mathbf{k}, \omega) \mathrm{d}\mathbf{k} \mathrm{d}\tilde{\mathbf{k}} \right]. \tag{14}$$

The sensitivity function of the sound pressure in the wavenumber domain is related to the sensitivity function of the the particle velocity at the panel surface as follows [23]

$$\tilde{H}_p(\tilde{\mathbf{k}}, \mathbf{k}, \omega) = \frac{\rho_f \omega}{\tilde{k}_z(\tilde{\mathbf{k}})} \tilde{H}_{v_f}(\tilde{\mathbf{k}}, \mathbf{k}, \omega) \tag{15}$$

where

$$\tilde{k}_z(\tilde{\mathbf{k}}) = \left\{ \begin{array}{ll} \sqrt{k_f^2 - \tilde{k}_x^2 - \tilde{k}_y^2}, & k_f^2 \geq \tilde{k}_x^2 + \tilde{k}_y^2 \\ \mathrm{i}\sqrt{\tilde{k}_x^2 + \tilde{k}_y^2 - k_f^2}, & \text{otherwise} \end{array} \right\}, \tag{16}$$

and k_f is the acoustic wavenumber, ρ_f is the fluid density, and $\tilde{\mathbf{k}} = (\tilde{k}_x, \tilde{k}_y)$. Substituting equation (15) in equation (14), the radiated acoustic power becomes

$$\Pi_{\mathrm{rad}}(\omega) = \mathrm{Re}\left[\frac{\rho_f \omega}{16\pi^4} \int\limits_{\infty}^{} \int\limits_{\infty}^{} \frac{1}{\tilde{k}_z(\tilde{\mathbf{k}})} \left| H_{v_f}(\tilde{\mathbf{k}}, \mathbf{k}, \omega) \right|^2 \phi_{pp}(\mathbf{k}, \omega) \mathrm{d}\tilde{\mathbf{k}} \mathrm{d}\mathbf{k} \right]. \tag{17}$$

According to equation (16), when the wavenumbers are outside the acoustic circle defined by $\Omega_a = \left\{ \tilde{\mathbf{k}} \in \mathbb{R}^2, \left| \tilde{\mathbf{k}} \right| \leq k_f \right\}$, $\tilde{k}_z(\tilde{\mathbf{k}})$ becomes purely imaginary. As such, only wavenumbers inside the acoustic circle contribute to the radiated acoustic power. Hence equation (17) can be rewritten as

$$\Pi_{\mathrm{rad}}(\omega) = \frac{\rho_f \omega}{16\pi^4} \int\limits_{\infty}^{} \int\limits_{\tilde{\mathbf{k}} \in \Omega_a}^{} \frac{1}{\sqrt{k_f^2 - \tilde{k}_x^2 - \tilde{k}_y^2}} \left| H_{v_f}(\tilde{k}_x, \tilde{k}_y, \mathbf{k}, \omega) \right|^2 \phi_{pp}(\mathbf{k}, \omega) \mathrm{d}\tilde{\mathbf{k}} \mathrm{d}\mathbf{k}. \tag{18}$$

In equation (18), the term in the denominator becomes zero for wavenumbers on the acoustic circle. This singularity is analytically removed in what follows. Using the following conversion formulas

$$\tilde{k}_x = \tilde{k}_r \, \sin\theta; \qquad \tilde{k}_y = \tilde{k}_r \, \cos\theta, \tag{19}$$

equation (18) can be transformed to polar wavenumber coordinates as follows

$$\Pi_{\mathrm{rad}}(\omega) = \frac{\rho_f \omega}{16\pi^4} \int\limits_{\infty}^{} \left(\int_{\theta=0}^{\theta=2\pi} \int_{\tilde{k}_r=0}^{\tilde{k}_r=k_f} \frac{\tilde{k}_r}{\sqrt{k_f^2 - \tilde{k}_r^2}} \right. \tag{20}$$

$$\left. \left| H_{v_f}(\tilde{k}_r \, \sin\theta, \tilde{k}_r \, \cos\theta, \mathbf{k}, \omega) \right|^2 \mathrm{d}\tilde{k}_r \mathrm{d}\theta \right) \phi_{pp}(\mathbf{k}, \omega) \mathrm{d}\mathbf{k}.$$

Finally, the change of variable, $\tilde{k}_r = k_f \, \sin\gamma$ analytically removes the singularity from the integral. As such, equation (20) can be expressed by

$$\Pi_{\mathrm{rad}}(\omega) = \frac{\rho_f k_f \omega}{16\pi^4} \int\limits_{\infty}^{} \left(\int_{\theta=0}^{\theta=2\pi} \int_{\gamma=0}^{\gamma=\frac{\pi}{2}} \sin\gamma \right. \tag{21}$$

$$\left. \left| H_{v_f}(k_f \, \sin\gamma\sin\theta, k_f \, \sin\gamma\cos\theta, \mathbf{k}, \omega) \right|^2 \mathrm{d}\gamma \mathrm{d}\theta \right) \phi_{pp}(\mathbf{k}, \omega) \mathrm{d}\mathbf{k}.$$

Employing the rectangular method for the numerical integration in equation (21), the radiated acoustic power becomes

$$\Pi_{\text{rad}}(\omega) = \frac{\rho_f k_f \omega}{16\pi^4} \sum_{-\mathbf{k}_{\text{cut-off}}}^{\mathbf{k}_{\text{cut-off}}} \left(\sum_{\theta\in[0,2\pi]} \sum_{\gamma\in[0,\frac{\pi}{2}]} \sin\gamma \right. \\ \left. \left| H_{v_f}(k_f \sin\gamma \sin\theta, \tilde{k}_r \cos\theta, \mathbf{k}, \omega) \right|^2 \phi_{pp}(\mathbf{k}, \omega) \delta\gamma \delta\theta \right) \delta\mathbf{k}, \tag{22}$$

where $\mathbf{k}_{\text{cut-off}}$ is cut-off wavenumber and $\delta\gamma$, $\delta\theta$, $\delta\mathbf{k}$ are the increments in the numerical integration. The sensitivity function H_{v_f} is given in Appendix A for a simply supported panel.

3. Numerical formulation

In the numerical formulation, the uncorrelated wall plane wave (UWPW) technique recently introduced by Maxit [21] is used to simulate the WPF generated by the TBL. The WPF generated by the TBL is represented by a set of deterministic pressure fields at each frequency of interest. Each realisation of the pressure field is applied as a deterministic input load to an element-based vibroacoustic solver. The structural and acoustic responses of the panel are then obtained for an ensemble average of the different panel responses at each frequency. This approach provides efficient coupling between the statistical model to describe the wall pressure fluctuations and the deterministic model to describe the panel vibroacoustic responses. The pressure beneath the TBL for the l^{th} realisation can be represented by a set of UWPWs at the q^{th} node of an FEM mesh as follows [9; 21; 25]

$$p^l_{\text{inc}}(\mathbf{x}^q, \omega) = \sum_{i=1}^{N_x} \sum_{j=1}^{N_y} \sqrt{\frac{\phi_{pp}(k^i_x, k^j_y, \omega) \delta k_x \delta k_y}{4\pi^2}} e^{\mathrm{i}(k^i_x x^q + k^j_y y^q + \varphi^l_{ij})}, \tag{23}$$

where φ is a random phase uniformly distributed in $[0\ \ 2\pi]$. The CSD can be expressed in terms of the ASD of the pressure field $S_{pp}(\omega)$ and the normalized CSD of the pressure field $\tilde{\phi}_{pp}(\mathbf{k}, \omega)$ as follows [21; 26]

$$\phi_{pp}(\mathbf{k}, \omega) = S_{pp}(\omega) \left(\frac{U_c}{\omega} \right)^2 \tilde{\phi}_{pp}(\mathbf{k}, \omega), \tag{24}$$

where U_c is the convective velocity. Using equation (23) as the deterministic load, the FEM is now implemented to simultaneously compute the l^{th} realisation of the structural displacement $\mathbf{u}^l$ and the radiated pressure $\mathbf{p}^l$ by solving the following fully coupled structural-acoustic equations [27]

$$\underbrace{\begin{bmatrix} -\omega^2\mathbf{M}_s + \mathbf{K}_s & -\mathbf{H}_{fs} \\ -\omega^2\rho_f c_f^2 \mathbf{H}_{fs}^{\mathrm{T}} & -\omega^2\mathbf{M}_f + \mathbf{K}_f \end{bmatrix}}_{\mathbf{A}} \begin{bmatrix} \mathbf{u}^l \\ \mathbf{p}^l \end{bmatrix} = \begin{bmatrix} \mathbf{f}_s^l \\ \mathbf{f}_f \end{bmatrix}, \tag{25}$$

where $\mathbf{K}$, $\mathbf{H}$ and $\mathbf{M}$ are respectively stiffness, coupling and mass matrices. Subscripts s and f respectively refer to the structure and fluid. $\mathbf{f}_s^l$ is the structural force vector corresponding to the l^{th} realisation of the TBL pressure field given by equation (23). $\mathbf{f}_f$ is the load from acoustic sources in the fluid domain, which is zero for the current case. After the inverse of the coefficient matrix $\mathbf{A}$ is obtained, the panel displacement response and radiated pressure can be computed for each realisation as follows

$$\begin{bmatrix} \mathbf{u}^l \\ \mathbf{p}^l \end{bmatrix} = \mathbf{A}^{-1} \begin{bmatrix} \mathbf{f}_s^l \\ \mathbf{0} \end{bmatrix}. \tag{26}$$

The ASD of the panel vibration velocity S_{vv} and the cross spectrum between the sound pressure and the fluid particle velocity S_{pv_f} due to the TBL excitation is then calculated from the ensemble average of the different realisations by

$$S_{vv} = -\omega^2 \mathrm{E}\left[\mathbf{u}^l \mathbf{u}^{*l}\right]_l, \tag{27}$$

$$S_{pv_f} = \mathrm{E}\left[\mathbf{p}^l \mathbf{v}_{\mathbf{f}}^{*l}\right]_l, \tag{28}$$

where $\mathrm{E}[\ ]$ represents the ensemble average of the realisations. This process is repeated for each frequency to obtain the spectra of the structural response. The method described here is termed the hybrid UWPW-FEM approach, whereby the UWPW technique was used to describe the WPF and a structural-acoustic solver based on the FEM method was employed to compute the vibroacoustic responses. It is worth noting that any element based approach can be used to obtain vibroacoustic responses of the panel. For example, instead of a coupled FEM-FEM model for the vibroacoustic solver as used in this work, a coupled finite element/boundary element method (FEM-BEM) can be employed to predict the vibroacoustic responses of the panel.

4. Results and discussion

A rectangular baffled aluminium panel with simply-supported boundary conditions and excited by a TBL is examined. The aluminium panel of dimensions 0.6 × 0.525 m^2 and 2.4 mm thickness was located in a 1.22 × 2.44 m^2 rigid panel made of medium density fibreboard of thickness 19 mm, as shown in Figure 2(a). Fabrication of the simply-supported boundary conditions for the experimental set-up of the aluminium test panel is described in [28]. The panel was tested in an anechoic wind tunnel at the Université de Sherbrooke [29]. The edge of the panel was placed 1.8 m from the convergent. To help with the development of the TBL, a sandpaper strip was glued at the intersection of the convergent and rigid baffle. This also removed any discontinuity at the intersection of the baffle and the convergent. To reduce the flanking transmission paths from the baffle, the test panel was decoupled from the baffle and positioned on its own supporting stand. Sound absorbing material was also placed on the stand to diminish possible sound reflections (for more information on the characteristic of the absorbing material, see [30]). The measurement space below the panel was acoustically treated using rigid tiles made of perlite-felt mix and backed by panels of compressed 0.0254 m thick glasswool.

The experiments were conducted at a free flow speed of 40 m/s. The boundary layer was developed on an extended flat surface in a low Mach number flow with zero pressure gradient. In such a flow condition, the boundary layer thickness increased slowly in the flow direction as such the TBL can be assumed as a homogeneous spatial field and stationary in time. The panel mean quadratic velocity was computed from 20 discrete measurement points using an array of accelerometers as described in [29]. To measure the radiated sound, a shoebox-shaped microphone array was employed in accordance with ISO3744 [31]. The array comprised 48 microphones placed along a parallelepiped measurement surface and was located below the panel in an acoustically treated box, as shown in Figure 2(b). The floor of the measurement space was opened towards the anechoic room. The grid floor was covered with compressed fibreglass panels. The stand of the test panel was also covered by sound insulation material.

The wall pressure fluctuations of the turbulent flow generated over the baffle were measured with a flush-mounted microphone array as described in [6; 29]. The Mellen model was fitted to the measured WPF using the least square method to estimate the decay rates, α_x and α_y, and the convective

velocity U_c. Using the experimentally fitted Mellen model and the measured ASD of the wall pressure presented in Appendix B, the CSD of the WPF was evaluated using equation (24) and used for all proceeding analytical and numerical results.

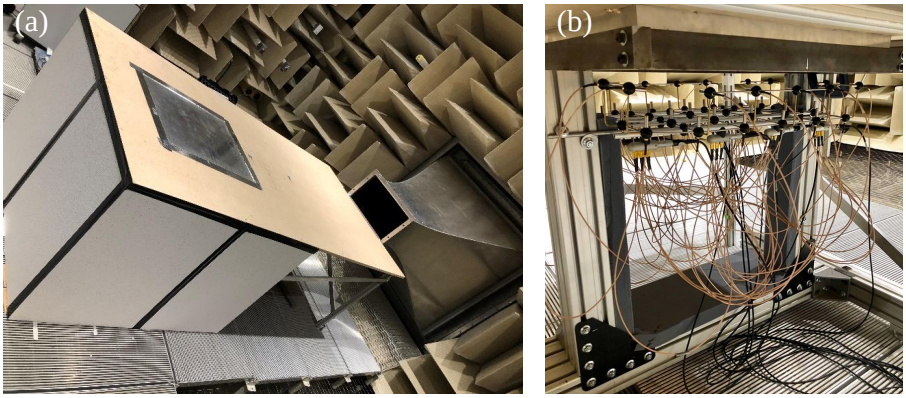

Figure 2: (a) Experimental set-up of the simply supported baffled rectangular plate in the anechoic wind tunnel at the Université de Sherbrooke [29], (b) parallelepiped microphone array used for the measuring radiated sound pressure.

Analytical results obtained using the sensitivity functions as well as numerical results obtained using the hybrid UWPW-FEM technique are compared with the experimental data obtained in an anechoic wind tunnel [29]. The dimensions and material properties of the panel are listed in Table 1. The fluid density and kinematic viscosity were set to 1.225 kg/m^3 and 1.511 $\times$ 10^{-5} m^2/s, respectively. The structural loss factor was experimentally estimated using the -3dB bandwidth method for the first ten resonances of the plate. The mean value of the loss factors was used in the analytical and numerical models. The simulations were conducted using Matlab on a desktop personal computer with 32 GB of RAM and a total of four physical cores. For the UWPW-FEM technique, the wall pressure field was synthesized in Matlab and then imported as a load to an FEM model of the panel and acoustic domain in the commercial software COMSOL Multiphysics (v5.3a) using Matlab LiveLink. The acoustic domain in the FEM model was modelled using the Pressure Acoustics module and was discretised using tetrahedral elements. The panel was modelled using the Shell Interface in the Structural Mechanics module and was meshed using structured quadrilateral

Table 1. Dimensions and material properties of the panel

Parameter	Value
Young's modulus, E (GPa)	68.9
Poisson's ratio, ν	0.3
Mass density, ρ_s (kg/m^3)	2740
Length, L_x (mm)	600
Width, L_y (mm)	525
Thickness, h_s (mm)	2.4
Damping loss factor, η	0.01

elements. The Acoustic-Structure Boundary coupling was applied to couple the acoustic domain to the panel. The MUMPS (MUltifrontal Massively Parallel Sparse) direct solver was employed with the memory allocation factor of 1.2 [32].

Figure 3 illustrates the FEM model of the panel and acoustic domain. The anechoic chamber located below the panel in the experiment was simulated using a hemisphere with a radius of 600 mm as shown in Figure 3. A perfectly matched layer (non-reflecting boundary condition) was applied on the boundary of the acoustic domain to allow the outgoing sound waves to leave the domain with minimal reflections. Similar to the experimental set-up, a rigid baffle was implemented. The 3D acoustic domain in the FE model was discretised using tetrahedral elements.

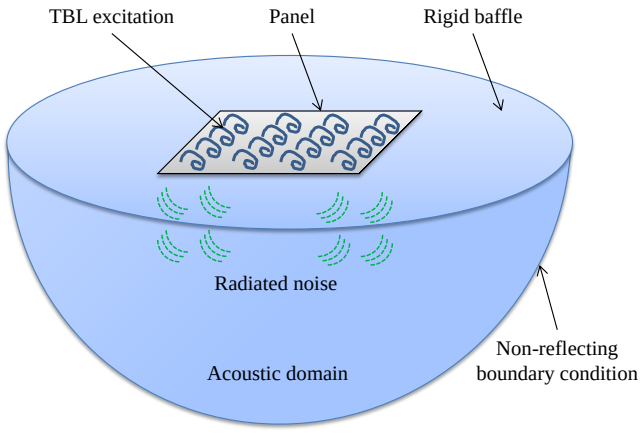

Figure 3: Schematic diagram of the FEM computational domain.

To obtain the panel response analytically and numerically, truncation of the wavenumber domain is required, whereby a truncated number of wavenumbers in the x and y directions need to be defined for equations (22) and (23). The criterion for defining the cut-off wavenumbers in the streamwise and spanwise directions must be chosen such that the significant contributions of the integrands of these equations are correctly taken into account. For frequencies well above the aerodynamic coincidence frequency, it has been previously demonstrated that for prediction of the panel vibrational response, wavenumbers below or close to the flexural wavenumber of the plate are dominant [1; 6; 21]. A cut-off wavenumber of $\mathbf{k}_{\text{cut-off}} = \{2k_{p,\max}, 2k_{p,\max}\}$ was used in both the streamwise and spanwise directions, where $k_{p,\max} = (\omega_{\max}\sqrt{\rho_s h/D})^{1/2}$ is the flexural wavenumber of the plate at the maximum frequency of interest denoted by $\omega_{\max}$. The wavenumber resolutions were set to $\delta k_x = \delta k_y = 0.25$ (1/m). The following criterion was used for the mesh size to take into account spatial variation of the WPF and to properly resolve structural modes

$$\Delta x = \Delta y = \min\left\{\frac{\lambda_{p,\max}}{10}, \frac{\pi}{2k_{p,\max}}\right\} = \frac{\lambda_{p,\max}}{10}, \tag{29}$$

where Δx, Δy are the element size in the x and y directions and $\lambda_{p,\max}$ is the flexural wavelength of the plate at the maximum frequency of interest. In equation (22), $\delta\gamma = \pi/100$, $\delta\theta = \pi/50$ were used to numerically evaluate the acoustic power. A frequency resolution of 1 Hz was used in all numerical simulations.

4.1. Structural response of the panel

The UWPW technique described in Section 3 was used to synthesize the pressure field on the surface of the panel. Figure 4 shows the visualization of a single realisation of the surface pressure field at two discrete resonance frequencies corresponding to 224 Hz and 416 Hz, for a flow speed of 40 m/s. From Figure 4 it can be observed that at 416 Hz, a slightly higher spatial resolution is needed to properly describe and synthesize the WPF for plane waves compared to that needed at the lower frequency of 224 Hz. Figure 5 presents the panel displacement at the two discrete frequencies using the single realisation of the WPF shown in Figure 4, and 30 realisations of the WPF. At the frequencies considered here, 30 realisations of the WPF are sufficient to obtain a converged solution. The converged panel displacement fields in Figure 5 reveals that the selected resonance frequencies correspond

to mode (m, n)=(3,2) at 224 Hz and (m, n)=(5,1) at 416 Hz. The effect of the number of realisations on the structural response of the panel is shown in Figure 6. Results for the velocity spectrum obtained analytically are also shown. An excellent match between the numerical and analytical results can be observed. Using 30 realisations, the maximum estimated error in the calculation of the panel response was less than 1 dB for the frequency range considered here. As such, 30 realisations were used for all subsequent calculations.

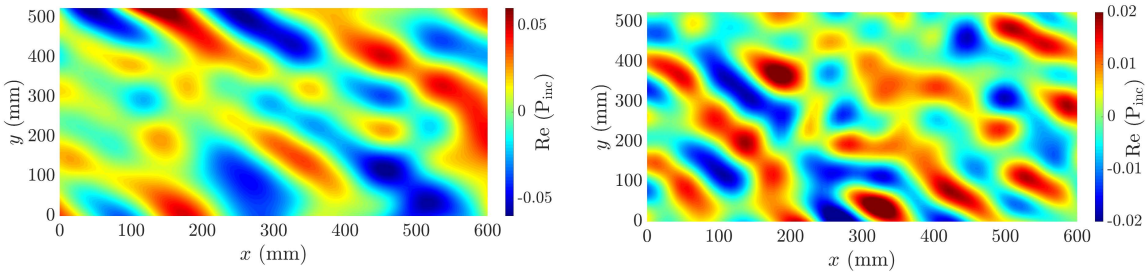

(a) **(b)**

Figure 4: A single realisation of the wall pressure field for a flow speed of 40 m/s at (a) 224 Hz and (b) 416 Hz.

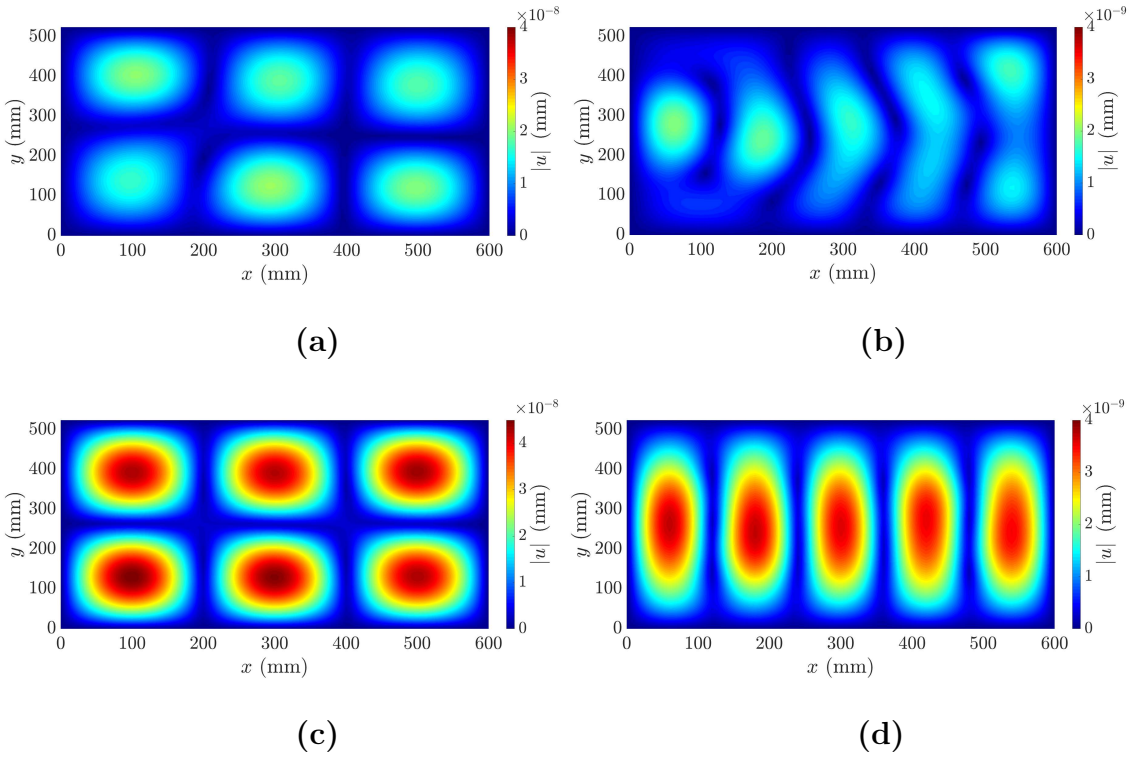

Figure 5: Panel displacement for a flow speed of 40 m/s at 224 Hz (a,c) and 416 Hz (b,d) using (a,b) a single realisation of the WPF corresponding to the WPF shown in Figure 4, and (c,d) the ensemble average of 30 realisations of the WPF.

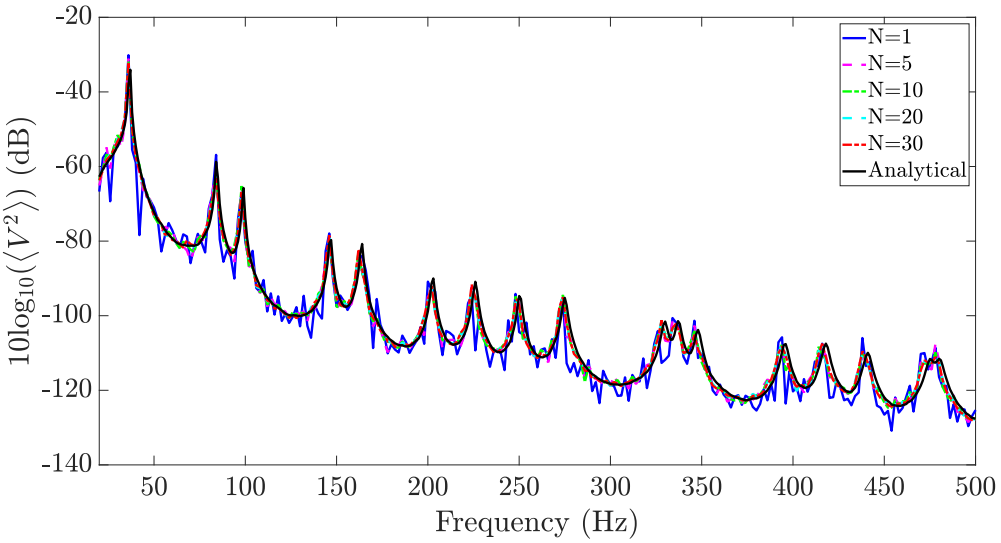

Figure 6: Predicted mean quadratic velocity spectra using different number of realisations at a flow velocity of $U_\infty = 40$ m/s (dB ref. 1 $(\mathrm{m/s})^2/\mathrm{Hz}$).

Figure 7 compares the velocity spectra predicted analytically and numerically with experimental data. Very close agreement between predicted and measured results can be observed, with only a slight shift in resonance frequencies attributed to potential differences in the panel material properties and implementation of the boundary conditions. The TBL excitation strongly excites the structure at the aerodynamic coincidence frequency, f_c, which occurs when the flexural wavenumber given by $k_p = (\omega\sqrt{\rho_s h/D})^{1/2}$ is equal to the convective wavenumber $k_c = \omega/U_c$, that is, $f_c = U_c^2\sqrt{\rho_s h/D}/(2\pi)$ [6]. For the parameters chosen here and at a flow speed of 40 m/s, f_c=39 Hz and is close to the first resonance of the plate.

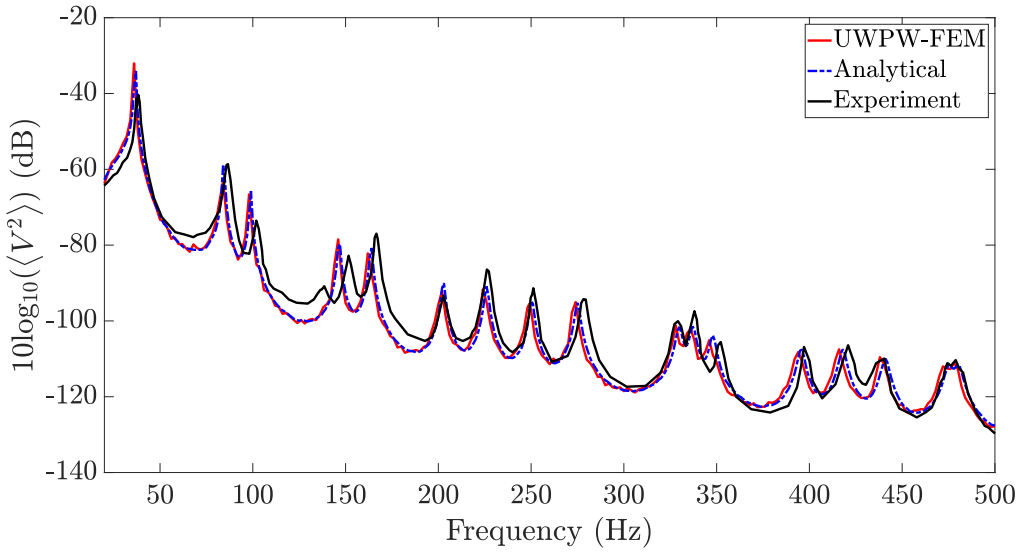

Figure 7: Predicted and measured mean quadratic velocity spectra at a flow velocity of $U_\infty = 40$ m/s (dB ref. 1 $(\mathrm{m/s})^2/\mathrm{Hz}$).

4.2. Acoustic response of the panel

It was already confirmed that for predicting structural response of a panel excited by TBL the cut-off wavenumber can be defined based on the flexural wavenumber and the effect of convected ridge can be neglected [9]. In this section, the validity of this criterion for evaluation the acoustic response of the panel is examined. To do this, the radiated acoustic power was obtained using a very large cut-off wavenumber (two times the convective wavenumber at the highest frequency of interest), as well as by using a cut-off wavenumber based on the flexural wavenumber. A maximum difference less than 0.5 dB was observed (results are not shown here), attributed to the filtering effect of the structure. This effect can be illustrated by plotting the forcing function and sensitivity function. To do this, equation (21) can be further written in a compact form as follows

$$\Pi_{\mathrm{rad}}(\omega) = \mathrm{Re}\left[\left(\frac{1}{4\pi^2}\right)\int_{\infty} \left|\tilde{H}_{\Pi}(\mathbf{k},\omega)\right|^2 \phi_{pp}(\mathbf{k},\omega)\mathrm{d}\mathbf{k}\right], \tag{30}$$

where $\left|\tilde{H}_{\Pi}(\mathbf{k},\omega)\right|$ is the acoustic power sensitivity function given by

$$\left|\tilde{H}_{\Pi}(\mathbf{k},\omega)\right|^2 = \frac{\rho_f k_f \omega}{4\pi^2}\left(\int_{\theta=0}^{\theta=2\pi}\int_{\gamma=0}^{\gamma=\frac{\pi}{2}} \sin\gamma \left|H_{v_f}(k_f\ \sin\gamma\sin\theta, k_f\ \sin\gamma\cos\theta, \mathbf{k}, \omega)\right|^2 \mathrm{d}\gamma\mathrm{d}\theta\right). \tag{31}$$

Figure 8(a) shows a map of the acoustic power sensitivity function. The white dashed lines correspond to the plate flexural wavenumbers. The maximum values for the sensitivity function occur at wavenumbers smaller than or close to the flexural wavenumbers. However, the magnitude of the function is still significant for those wavenumbers larger than the flexural wavenumbers. Figure 8(b) presents the TBL forcing function, corresponding to the CSD of the WPF. The dash-dotted line corresponds to the convective wavenumbers where the TBL excitation is strong. The filtering effect of the structure is illustrated in Figure 8(c), which presents the product of the sensitivity function and forcing function. It can be observed that the structure filters out most of the wavenumbers larger than flexural wavenumbers. Only wavenumbers smaller than flexural wavenumbers contribute to the radiated acoustic power. However below 300 Hz, the effect of the convective ridge was not completely filtered by the panel. Whilst this contribution is not significant, the effect of the convective ridge was taken into account here as the cut-off wavenumber was defined as twice the flexural wavenumber at the highest frequency of interest.

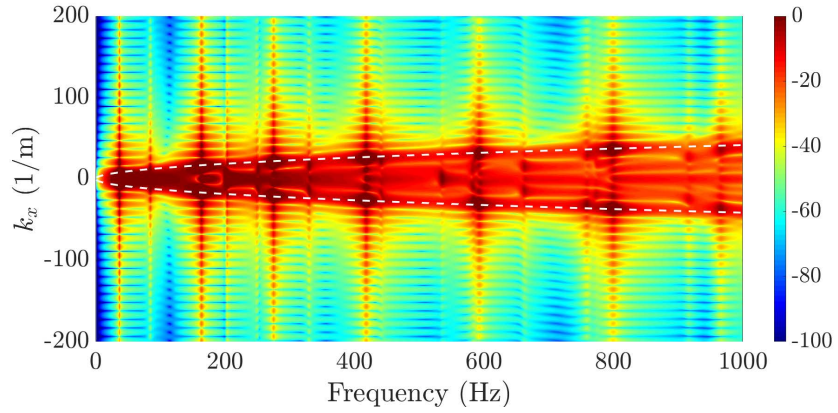

(a)

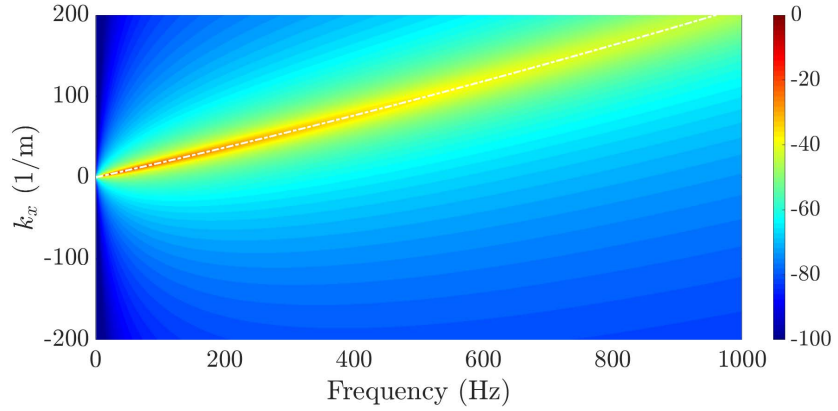

(b)

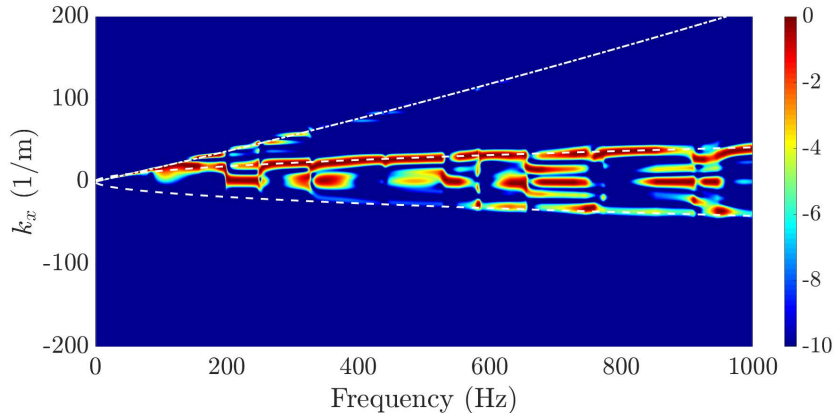

(c)

Figure 8: Maps of the (a) acoustic power sensitivity functions, $\left|\tilde{H}_{\Pi}(\mathbf{k},\omega)\right|^2$ (dB, ref. $\mathrm{Pa}^{-1}\mathrm{m}^3\mathrm{s}^{-2}\mathrm{rad}^2$), (b) CSD function of the wall pressure spectrum using the Mellen and measured ASD function, $\phi_{pp}(\mathbf{k},\omega)$ (dB, ref. 1 $\mathrm{Pa}^2\mathrm{m}^2\mathrm{s\ rad}^{-2}$), and (c) result obtained by the product of (a) and (b) (dB, ref. 1 Wm^2). The dashed lines in (a) and (c) correspond to the plate flexural wavenumber; the dashed-dot line in (b) and (c) corresponds to the convective wavenumber.

The absolute radiated pressure from the panel at the two discrete resonance frequencies of 224 Hz and 416 Hz is shown in Figure 9, using the single realisation of the wall pressure (Figures 9(a) and (b)) as well as 30 realisations of the WPF (Figures 9(c) and (d)). A converged solution for the pressure fields is obtained using 30 realisations of the WPF. This was verified by comparing the numerical prediction of acoustic power with the analytical results as well as measured acoustic power in Figure 10. It can be seen that numerical results are in excellent agreement with analytical results. The predicted acoustic power is also in good agreement with the measured acoustic power. However, some discrepancies can be seen between predicted and measured acoustic power. It can be observed that the experimental data between resonance frequencies are relatively flat, this can be attributed to the effect of background noise in the wind tunnel. In fact TBL pressure fluctuations over the baffle generates noise which could be transmitted into the anechoic chamber located below the panel. This noise was not included in the simulation which may also explain the difference in magnitude between predicted and measured results. In addition, slight differences in implementing panel boundary conditions and material properties used in the numerical/analytical model and experiment can cause some discrepancies between the measured and radiated acoustic power. Although, there is a shift in frequency between numerical and experimental results in Figure 10, the predicted resonance frequencies correspond to those obtained from measurement. This was confirmed by comparing numerically calculated pressure distribution in a plane 100 mm below the panel with those obtained from the experiment using the microphone array as shown in Figure 11.

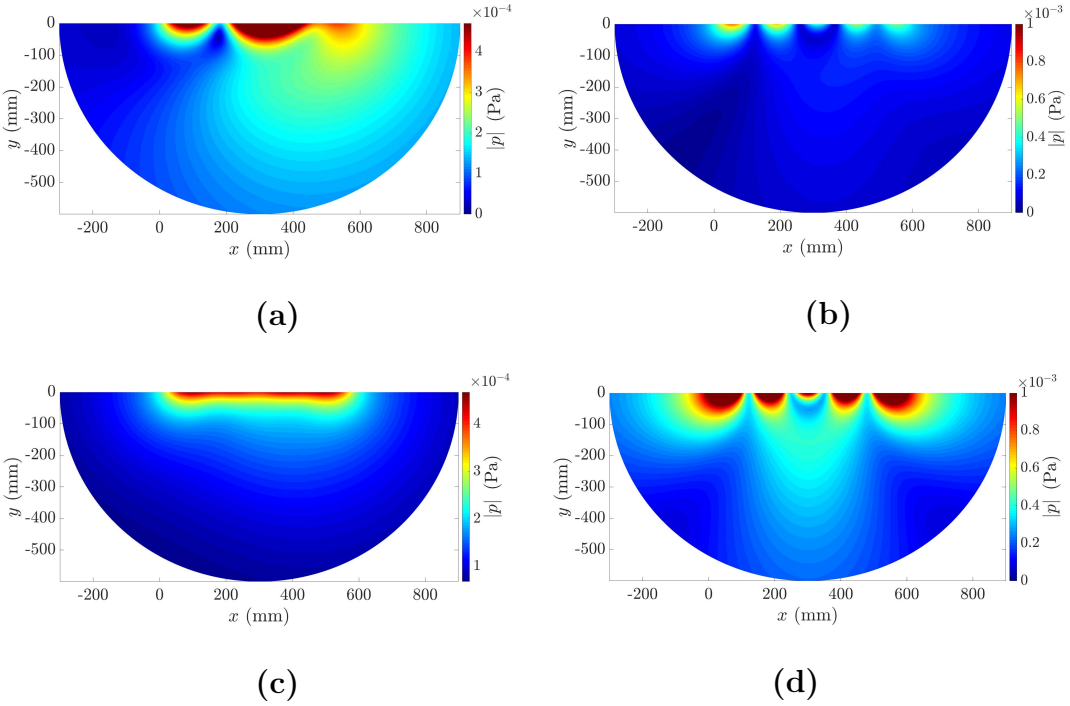

Figure 9: Pressure field in the xz-plane in the midspan of the panel at 224 Hz (a,c) and 416 Hz (b,d) using (a,b) a single realisation of the WPF corresponding to the WPF shown in Figure 4, and (c,d) the ensemble average of 30 realisations of the WPF.

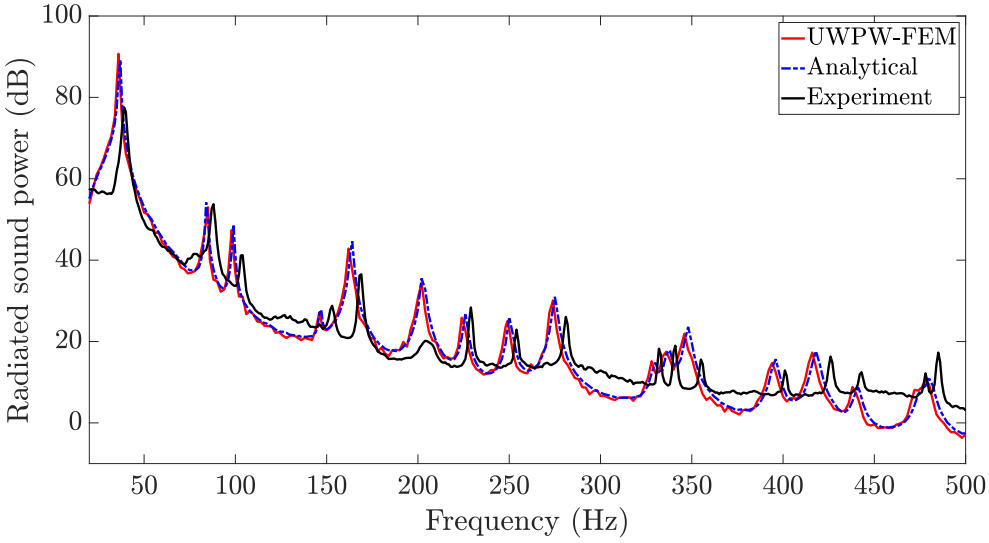

Figure 10: Predicted and measured acoustic power at flow velocity $U_\infty = 40$ m/s (dB ref. 1×10^{-12} (W)).

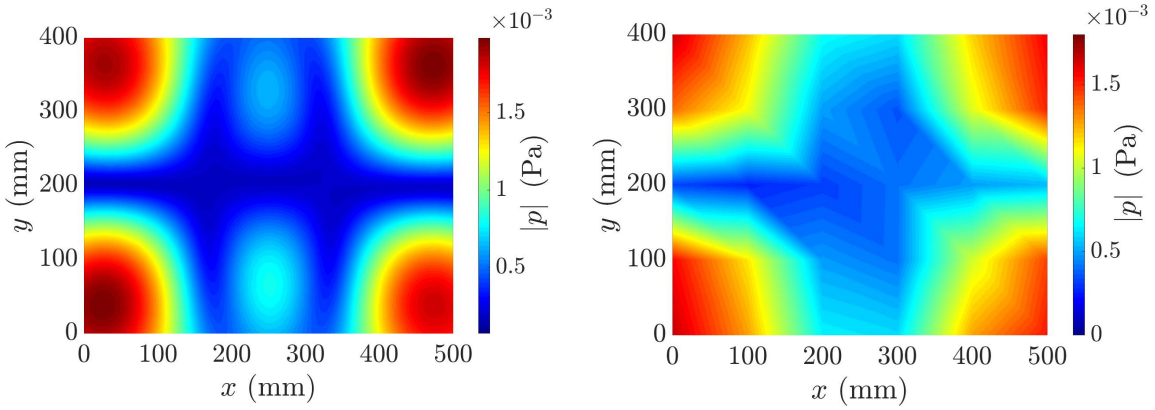

Figure 11: Maps of absolute radiated sound pressure in the xy-plane located 100 mm below the panel: (a) numerical results at 224 Hz; (b) experimental results at 229 Hz.

4.3. Application to a stiffened panel

To show one of the applications of the proposed numerical approach for complex panels, a simply supported stiffened panel is considered. Three stiffeners are added to the same panel considered in the previous section as shown in Figure 12. The stiffeners are located on the no-flow side of the panel. The cross-sectional dimensions of the stiffeners are 2.4 mm $\times$ 40 mm. The wavenumber characterizing the flexural motions of the stiffened panel is lower than that of the unstiffened panel as adding stiffeners increases panel stiffness. As such, the same cut-off wavenumber used for unstiffened panel could be used for the stiffened panel. Since the flow conditions and dimensions of stiffened panel are as same as those for unstiffened panel, there is no need to synthesize a new set of WPF, and the WPF generated using the UWPW technique in the previous section was used to predict the response of the stiffened panel. The stiffened panel is excited by TBL and its vibrational response and radiated acoustic power are compared with those obtained from the unstiffened panel as shown respectively in Figures 13 and 14. It was observed that stiffeners have significant effect on the vibroacoustic responses of the panel. The resonance frequencies of the stiffened panel are much higher than those of unstiffened panel, this is due to increase in panel stiffness by adding the stiffeners. At very low frequency (approximatively at 28 Hz) a hump can be seen in both Figures 13 and 14. This can be attributed to the aerodynamic coincidences frequency for the stiffened panel. This frequency was estimated for the unstiffened panel to be 39 Hz. Adding stiffeners increases the flexural rigidity of the panel which decreases the aerodynamic coincidences frequency. The peak appeared at frequency close to 260 Hz in structural and acoustic responses of the stiffened panel corresponds to a group of modes with resonance frequencies close to each other. This was examined using an eigen-frequency analysis of the stiffened panel. Presence of a group of modes in a narrow frequency band explains why the peak appeared at frequency close to 260 Hz is not as sharp as those occurs at single resonance frequency.

To examine the effect of stiffeners on acoustic radiation from the panel, the radiation efficiency of the panel is computed for both unstiffened and stiffened panels as shown in Figure 15. The radiation efficiency of a panel is given by

$$\sigma_{\text{rad}} = \frac{\Pi_{\text{rad}}}{A\rho_f c_f \langle V^2 \rangle}, \tag{32}$$

Figure 15 shows that except at very low frequencies, adding stiffeners increases radiation efficiency of the panel. This trend is well-known for panels excited by a single point force and it can also be observed here for panels excited by TBL excitation. Radiation efficiency is different for each mode. For a simply supported panel, it is well-known that odd-odd modes (means an odd mode in the x-direction and an odd mode in the y-direction) are the most efficient modes and even-even modes are the least efficient modes [33]. For example, at the resonance frequency around 150 Hz the unstiffened panel has very low radiation efficiency, this sharp trough corresponds to the mode number (2,2). In contrast, at frequency of approximately 200 Hz corresponding to the mode number (1,3) the panel efficiently radiates sound to the acoustic domain. As frequency increases both stiffened and unstiffened panels show an upward trend in the radiation efficiency. The results presented in this section highlights the capability of the proposed numerical approach to predict the vibroacoustic responses of complex panels under TBL excitation such as composite panels with stiffeners.

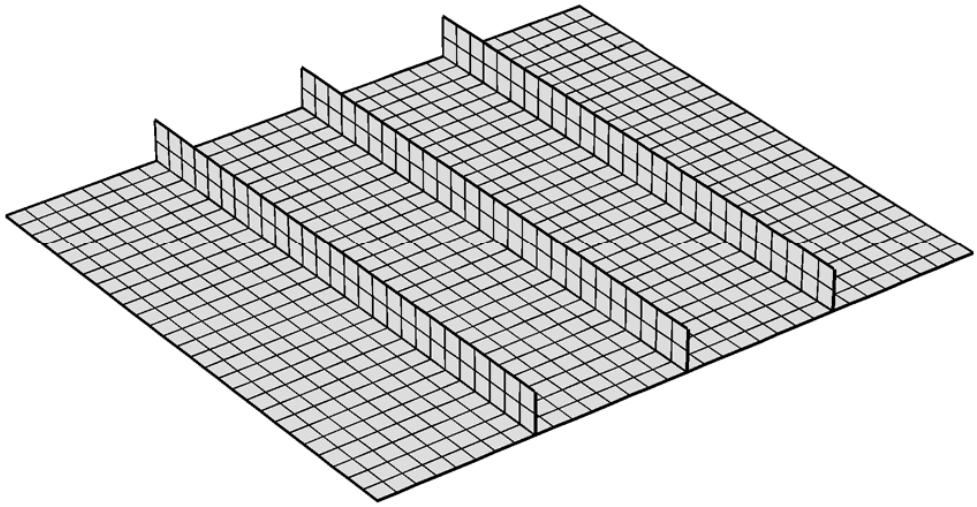

Figure 12: FEM model of the panel with three stiffeners oriented in spanwise direction.

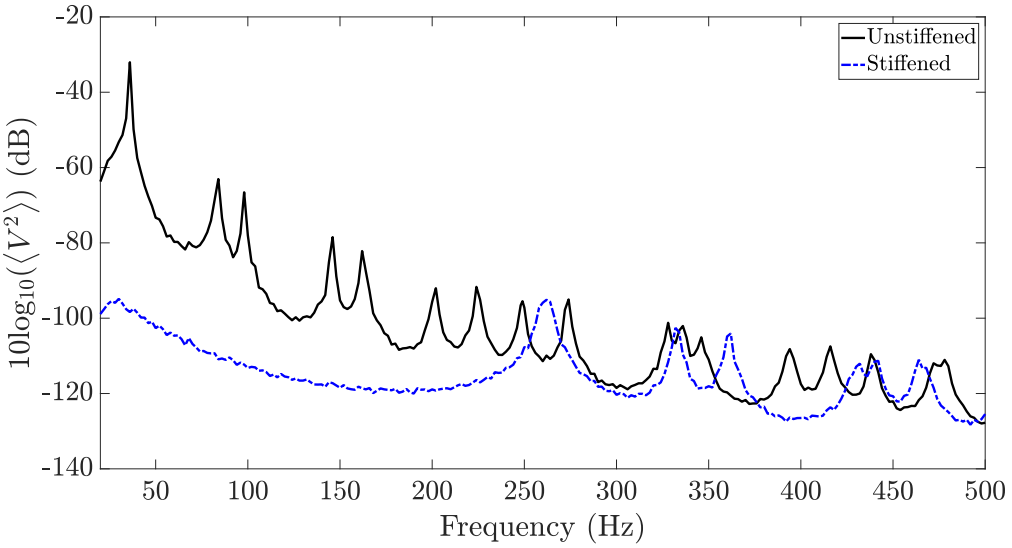

Figure 13: Predicted mean quadratic velocity spectra for unstiffened and stiffened panel, (dB ref. 1 $(\mathrm{m/s})^2/\mathrm{Hz}$).

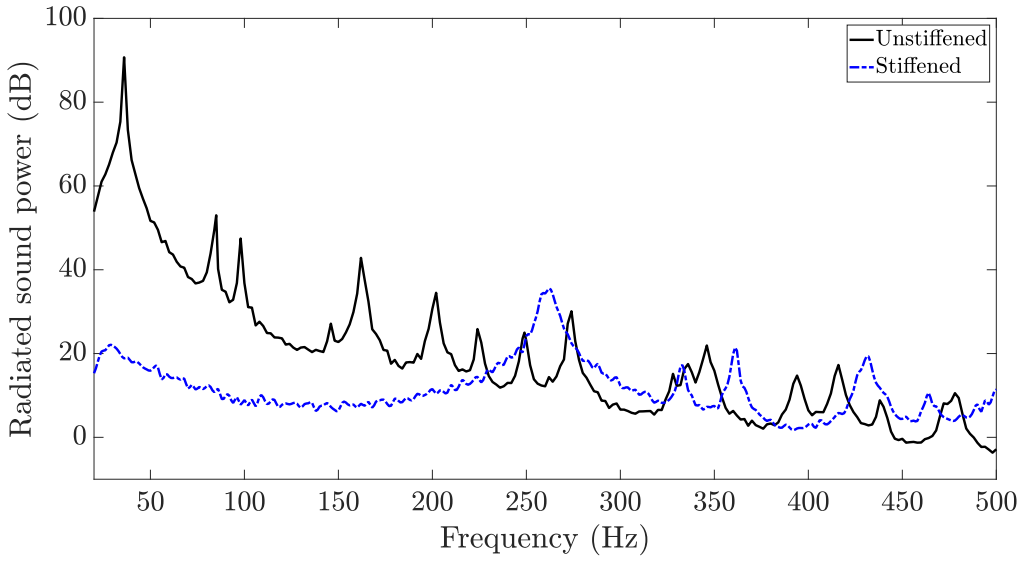

Figure 14: Predicted acoustic power for unstiffened and stiffened panel (dB ref. 1×10^{-12} (W)).

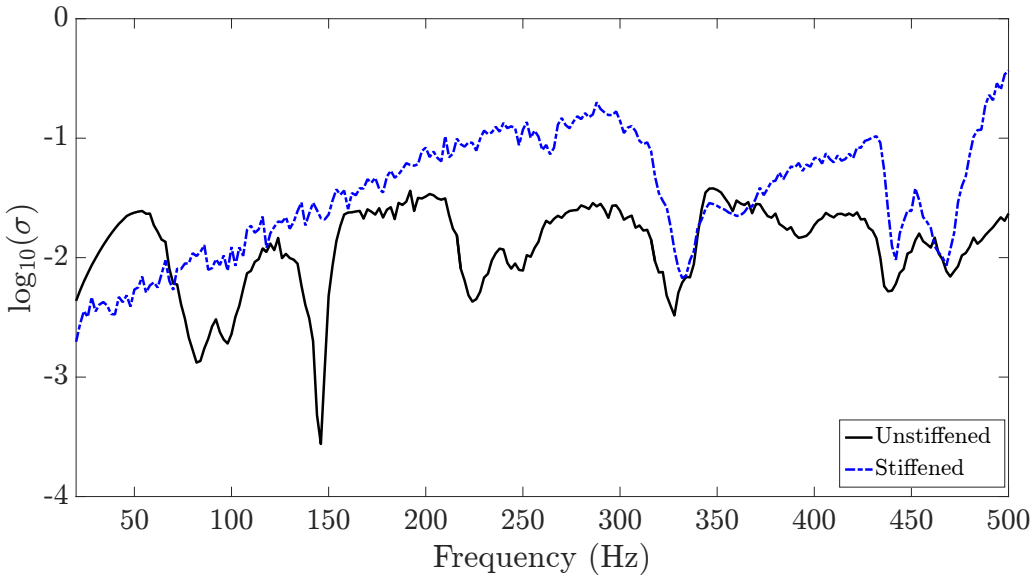

Figure 15: Radiation efficiency for stiffened and unstiffened panels.

5. Conclusions

The structural and acoustic responses of a simply supported panel under TBL excitation were numerically obtained using the hybrid UWPW-FEM approach. An analytical model based on sensitivity functions of the panel was used as a reference solution to verify the numerical method. Employing the acoustic power sensitivity functions, the effective wavenumber range for acoustic power calculation was identified and the filtering effect of the panel was illustrated. It was confirmed that both structural and acoustic responses of the panel can accurately be determined by choosing cut-off wavenumber based on the flexural wavenumber. The experimental data was also obtained from an anechoic wind tunnel to validate the numerical predictions. The numerical results were obtained by synthesizing the wall pressure field using the UWPW technique and applying different realisations of the WPF as deterministic loads to a fully coupled structural-acoustic solver based on the FEM. Since the WPF was obtained as deterministic loads, any element based methods such as the FEM and the boundary element method can be used for vibroacoustic calculation. Further, the proposed numerical approach can be applied to any complex planar structures with arbitrary boundary conditions. To illustrate one of the applications of the numerical approach, vibroacous-

tic responses of a stiffened panel subject to TBL excitation were studied. It was shown that adding stiffeners significantly increases the panel radiation efficiency. The main limitation of the proposed model corresponds to the accuracy in the simulation of the WPF. Errors in simulation of the WPF will inevitably result in errors in the prediction of the radiated acoustic pressure. Assumptions and limitations associated with the proposed model are (i) the TBL is homogeneous, stationary and fully developed over the structural surface in a subsonic flow, (ii) the influence of convection on the acoustic radiation from the structure is negligible, and (iii) the WPF is not altered by the vibration of the structure for which the fluid-structure interaction can be considered as weak coupling.

Acknowledgements

This research was supported by the Australian Government through the Australian Research Council's Discovery Early Career Project funding scheme (project DE190101412). The first author gratefully acknowledges travel fund from the LabEx CelyA of Université de Lyon for his research visit to INSA Lyon in France (ANR-10-LABX-0060/ANR-11-IDX-0007).

Appendix A

The sensitivity function $H_{v_s}(\mathbf{x}, \mathbf{k}, \omega)$ for a simply supported rectangular plate corresponding to the velocity at point $\mathbf{x}$ when the panel is excited by a unit wall plane wave is given by

$$H_{v_s}(\mathbf{x}, \mathbf{k}, \omega) = \mathrm{i}\omega \sum_{m=1}^{M} \sum_{n=1}^{N} \frac{\psi_{mn}(\mathbf{k})\varphi_{mn}(\mathbf{x})}{\Omega(\omega_{mn}^2 - \omega^2 + \mathrm{i}\eta\omega\omega_{mn})}, \tag{A.1}$$

$\Omega = \rho_s h L_x L_y/4$ is the modal mass. The modal frequencies are given by

$$\omega_{mn} = \sqrt{\frac{D}{\rho_s h}} \left((\frac{m\pi}{L_x})^2 + (\frac{n\pi}{L_y})^2 \right), \tag{A.2}$$

where $D = Eh^3/(12(1-\nu^2))$ is the flexural rigidity, E is the Young's modulus and ν is Poisson's ratio. The modal forces ψ_{mn} are calculated by integration over the panel surface as follows

$$\psi_{mn}(\mathbf{k}) = \int_A \varphi_{mn}(\mathbf{x}) e^{\mathrm{i}(k_x x + k_y y)} \mathrm{d}A = I_m^x(k_x) I_n^y(k_y), \tag{A.3}$$

where $\varphi_{mn}(\mathbf{x})$ are the panel mode shapes given by

$$\varphi_{mn}(\mathbf{x}) = \sin(\frac{m\pi x}{L_x})\sin(\frac{n\pi y}{L_y}), \tag{A.4}$$

and

$$\{I_s^r(k_r)|(r,s) = (x,m) \vee (y,n)\} = \left\{ \begin{array}{ll} \left(\frac{s\pi}{L_r}\right) \dfrac{(-1)^s e^{\mathrm{i}(k_r L_r)} - 1}{k_r^2 - \left(\frac{s\pi}{L_r}\right)^2}, & k_r \neq \frac{s\pi}{L_r} \\ \frac{1}{2}\mathrm{i}L_r, & \text{otherwise} \end{array} \right\} \tag{A.5}$$

At the interface between the plate and the acoustic domain, the structural velocity v_s is equal to fluid particle velocity v_f in the normal direction, that is $H_{v_f}(\mathbf{x},\mathbf{k},\omega) = H_{v_s}(\mathbf{x},\mathbf{k},\omega)$. As such, the sensitivity function $H_{v_f}(\tilde{\mathbf{k}},\mathbf{k},\omega)$ in equation (22) can be obtained analytically using a Fourier transform as follows

$$H_{v_f}(\tilde{\mathbf{k}},\mathbf{k},\omega) = \int_{\infty} H_{v_f}(\mathbf{x},\mathbf{k},\omega)e^{-\mathrm{i}\tilde{\mathbf{k}}\mathbf{x}}\mathrm{d}\mathbf{x} = \sum_{m=1}^{M}\sum_{n=1}^{N} a_{mn}(\tilde{\mathbf{k}},\omega)\psi_{mn}(\mathbf{k}), \tag{A.6}$$

where

$$a_{mn}(\tilde{\mathbf{k}},\omega) = \mathrm{i}\omega\frac{\psi_{mn}(-\tilde{\mathbf{k}})}{\Omega(\omega_{mn}^2 - \omega^2 + \mathrm{i}\eta\omega\omega_{mn})}, \tag{A.7}$$

and ψ_{mn} and I_s^r are given by equations (A.3)-(A.5).

Appendix B

The Mellen normalized wavenumber-frequency model is given by [34]

$$\tilde{\phi}_{pp}(k_x,k_y,\omega) = \frac{2\pi(\alpha_x\alpha_y)^2 k_{\mathrm{c}}^3}{\left((\alpha_x\alpha_y k_{\mathrm{c}})^2 + (\alpha_x k_y)^2 + \alpha_y^2\left(k_x - k_{\mathrm{c}}\right)^2\right)^{3/2}}, \tag{B.1}$$

where $k_c = \omega/U_c$. U_c, α_x and α_y were evaluated from experimental data as shown in Figure B1. The ASD of the WPF measured experimentally is shown in Figure B2.

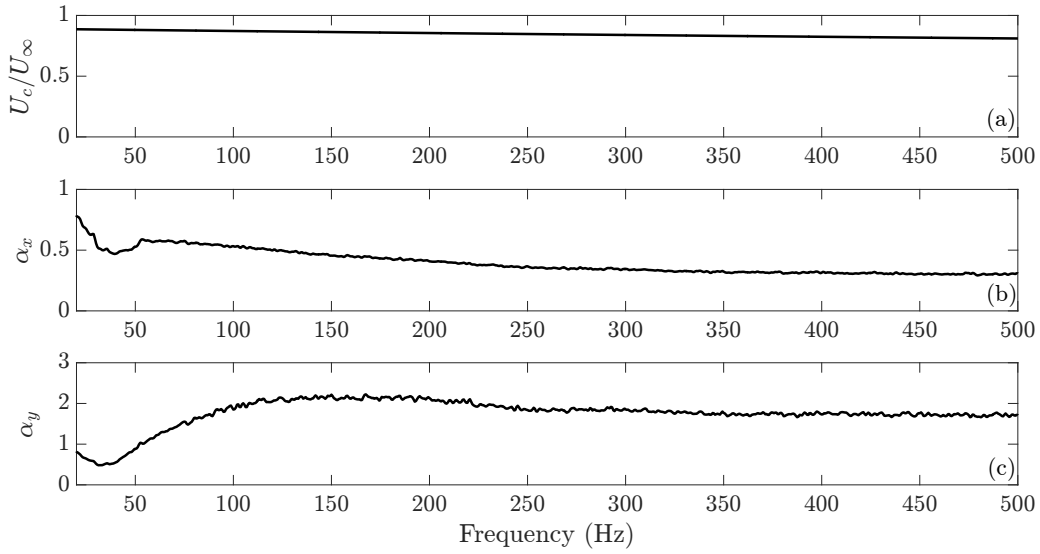

Figure B1: The TBL parameters extracted from measurements at $U_\infty = 40$ m/s: (a) convective speed normalized by the flow velocity; (b) streamwise exponential decay rate α_x; (c) spanwise exponential decay rate α_y.

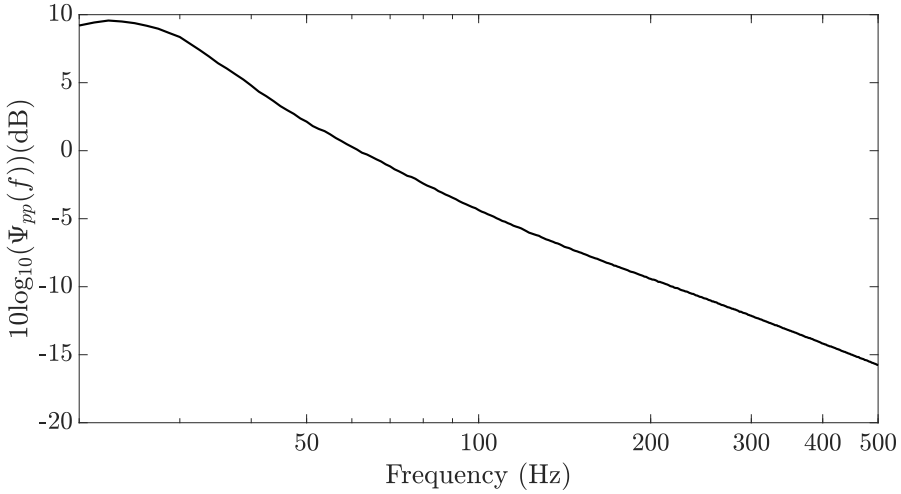

Figure B2: Measured ASD function of the wall pressure at $U_\infty = 40$ m/s (dB ref. 1 Pa^2/Hz).

References

[1] S. Hambric, Y. Hwang, W. Bonness, Vibrations of plates with clamped and free edges excited by low-speed turbulent boundary layer flow, J. Fluids. Struct. 19 (1) (2004) 93–110.

[2] S. De Rosa, F. Franco, Exact and numerical responses of a plate under a turbulent boundary layer excitation, J. Fluids. Struct. 24 (2) (2008) 212–230.

[3] D. Mazzoni, An efficient approximation for the vibro-acoustic response of a turbulent boundary layer excited panel, J. Sound. Vib. 264 (4) (2003) 951–971.

[4] B. Liu, L. Feng, A. Nilsson, M. Aversano, Predicted and measured plate velocities induced by turbulent boundary layers, J. Sound. Vib. 331 (24) (2012) 5309–5325.

[5] E. Ciappi, S. De Rosa, F. Franco, J. Guyader, S. Hambric, Flinovia - Flow Induced Noise and Vibration Issues and Aspects: A Focus on Measurement, Modeling, Simulation and Reproduction of the Flow Excitation and Flow Induced Response, EBL-Schweitzer, Springer International Publishing Switzerland, 2014.

[6] C. Marchetto, L. Maxit, O. Robin, A. Berry, Experimental prediction of the vibration response of panels under a turbulent boundary layer excitation from sensitivity functions, J. Acoust. Soc. Am. 143 (5) (2018) 2954–2964.

[7] E. Ciappi, S. De Rosa, F. Franco, J. Guyader, S. Hambric, R. Leung, A. Hanford, Flinovia-Flow Induced Noise and Vibration Issues and Aspects-II: A Focus on Measurement, Modeling, Simulation and Reproduction of the Flow Excitation and Flow Induced Response, Springer International Publishing Switzerland, 2018.

[8] Z. Xiaojian, A. Bangcheng, L. Ziqiang, L. Dun, A scaling procedure for panel vibro-acoustic response induced by turbulent boundary layer, J. Sound. Vib. 380 (2016) 165–179.

[9] M. Karimi, P. Croaker, L. Maxit, O. Robin, A. Skvortsov, S. Marburg, N. Kessissoglou, A hybrid numerical approach to predict the vibrational

responses of panels excited by a turbulent boundary layer, J. Fluids. Struct. 92 (2020) 102814.

[10] H. G. Davies, Sound from turbulent-boundary-layer-excited panels, J. Acoust. Soc. Am. 49 (3B) (1971) 878–889.

[11] F. Han, L. Mongeau, R. Bernhard, A model for the vibro-acoustic response of plates excited by complex flows, J. Sound. Vib. 246 (5) (2001) 901–926.

[12] C. Maury, P. Gardonio, S. Elliott, A wavenumber approach to modelling the response of a randomly excited panel, Part I: General theory, J. Sound. Vib. 252 (1) (2002) 83–113.

[13] C. Maury, P. Gardonio, S. Elliott, A wavenumber approach to modelling the response of a randomly excited panel, Part II: Application to aircraft panels excited by a turbulent boundary layer, J. Sound. Vib. 252 (1) (2002) 115–139.

[14] J. Rocha, Sound radiation and vibration of composite panels excited by turbulent flow: analytical prediction and analysis, Shock. Vib. 2014 (2014).

[15] C. Marchetto, L. Maxit, O. Robin, A. Berry, Vibroacoustic response of panels under diffuse acoustic field excitation from sensitivity functions and reciprocity principles, J. Acoust. Soc. Am. 141 (6) (2017) 4508–4521.

[16] Y. Kou, B. Liu, D. Chang, Radiation efficiency of plates subjected to turbulent boundary layer fluctuations, J. Acoust. Soc. Am. 139 (5) (2016) 2766–2771.

[17] G. Cousin, Sound from TBL-induced vibrations, in: 4th AIAA/CEAS Aeroacoustics Conference, Toulouse, France, 1998, p. 2216.

[18] J. Park, L. Mongeau, T. Siegmund, An investigation of the flow-induced sound and vibration of viscoelastically supported rectangular plates: experiments and model verification, J. Sound. Vib. 275 (1-2) (2004) 249–265.

[19] E. Ciappi, F. Magionesi, S. De Rosa, F. Franco, Hydrodynamic and hydroelastic analyses of a plate excited by the turbulent boundary layer, J. Fluids. Struct. 25 (2) (2009) 321–342.

[20] B. Liu, Noise radiation of aircraft panels subjected to boundary layer pressure fluctuations, J. Sound. Vib. 314 (3-5) (2008) 693–711.

[21] L. Maxit, Simulation of the pressure field beneath a turbulent boundary layer using realizations of uncorrelated wall plane waves, J. Acoust. Soc. Am. 140 (2) (2016) 1268–1285.

[22] D. E. Newland, An introduction to random vibrations, spectral & wavelet analysis, Courier Corporation, Mineola, New York, USA, 2012.

[23] E. G. Williams, Fourier acoustics: sound radiation and nearfield acoustical holography, Elsevier, San Diego, California, USA, 1999.

[24] C. Marchetto, Experimental characterization of the vibroacoustic response of panels under random excitations by sensitivity functions, Ph.D. thesis, Univ Lyon, INSA-Lyon, Laboratoire Vibrations-Acoustique (LVA), France (2018).

[25] M. Karimi, P. Croaker, A. Skvortsov, D. Moreau, N. Kessissoglou, Numerical prediction of turbulent boundary layer noise from a sharp-edged flat plate, Int. J. Numer. Meth. Fl. 90 (2019) 522–543.

[26] W. Graham, A comparison of models for the wavenumber–frequency spectrum of turbulent boundary layer pressures, J. Sound. Vib. 206 (4) (1997) 541–565.

[27] P. Davidsson, Structure-acoustic analysis; finite element modelling and reduction methods, Ph.D. thesis, Division of Structural Mechanics, LTH, Lund University, Lund, Sweden (2004).

[28] O. Robin, J.-D. Chazot, R. Boulandet, M. Michau, A. Berry, N. Atalla, A plane and thin panel with representative simply supported boundary conditions for laboratory vibroacoustic tests, Acta. Acust. united. Ac. 102 (1) (2016) 170–182.

[29] M. Jenzri, O. Robin, N. Atalla, Vibration of and radiated acoustic power from a simply-supported panel excited by a turbulent boundary layer excitation at low Mach number, Noise. Control. Eng. J. 67 (4) (2019) 241–251.

[30] O. Robin, A. Berry, C. Kafui Amédin, N. Atalla, O. Doutres, F. Sgard, Laboratory and in situ sound absorption measurement under a synthetized diffuse acoustic field, Build. Acoust. 26 (4) (2019) 223–242.

[31] International Organization for Standardization ISO3744. Acoustics - Determination of sound power levels and sound energy levels of noise sources using sound pressure - Engineering method in an essentially free field over a reflecting plane (2010).

[32] COMSOL Multiphysics Reference Manual, version 5.3a, COMSOL, Inc, www.comsol.com. (2017).

[33] Z. Dingguo, M. J. Crocker, Sound power radiated from rectangular plates, Arch. Acoust. 34 (1) (2009) 25–39.

[34] R. Mellen, Wave-vector filter analysis of turbulent flow, J. Acoust. Soc. Am. 95 (3) (1994) 1671–1673.